Three-dimensional Reconstruction of a Simple Z-band in Fish Muscle

Pradeep K. Luther

The Blackett Laboratory, Imperial College, London SW7 2BZ, England

Abstract. The three-dimensional structure of the Z-band in fish white muscle has been investigated by electron microscopy. This Z-band is described as simple, since in longitudinal sections it has the appearance of a single zigzag pattern connecting the ends of actin filaments of opposite polarity from adjacent sarcomeres. The reconstruction shows two pairs of links, the Z-links, between one actin filament and the facing four actin filaments in the adjacent sarcomere. The members of each pair have nearly diametrically opposed origins. In relation to one actin filament, one pair of links appears to bind along the final 10 nm of the actin filament (proximal site) and the other pair binds along a region extending from 5 to 20 nm from the filament end (distal site). Between one pair and the other, there is a rotation of ~80° round the filament axis. A Z-link with a proximal site at the end of one actin filament attaches at a distal site on the oppositely oriented actin filaments of the facing sarcomere and vice versa. The length of each Z-link is consistent with the length of an α-actinin molecule. An additional set of links located 10–15 nm from the center of the Z-band occurs between actin filaments of the same polarity. These polar links connect the actin filaments along the same direction on each side of the Z-band. The three-dimensional structure appears to have twofold screw symmetry about the central plane of the Z-band. Only approximate twofold rotational symmetry is observed in directions parallel to the actin filaments. Previous models of the Z-band in which four identical and rotationally symmetrical links emanate from the end of one actin filament and span across to the ends of four actin filaments in the adjacent sarcomere are therefore incorrect.

THE study of the Z-band in striated muscle is important as it helps us to understand how actin filaments from adjacent sarcomeres are anchored together. It is also important as it helps us to understand the interaction of actin with α-actinin, the main linking protein in the Z-band (Suzuki et al., 1976). The structural regularity in the Z-band in striated muscle makes it well suited for analyzing details of the three-dimensional (3D)[1] interaction of α-actinin and actin. At the Z-band an ordered array of actin filaments from one sarcomere interdigitates with the ordered array of oppositely oriented actin filaments from the adjacent sarcomere (Yamaguchi et al., 1983) and there are extensive cross-links between the two arrays, which are thought to be mainly due to α-actinin. There are now established methods of structure determination of periodic samples from electron micrographs (Amos et al., 1982; Luther and Crowther, 1984). These methods have recently been applied successfully for the honeybee Z-band (Cheng and Deatherage, 1989; Deatherage et al., 1989). The honeybee Z-band was found to be a highly complex structure, comprising interdigitating arrays of hexagonally arranged actin filaments overlapping by 80 nm with up to five different types of linkages between the actin filaments.

The Z-band architecture in vertebrate muscles, based on a tetragonal lattice, is inherently less complicated especially in narrow Z-bands. The width of the Z-band in longitudinal view, varies in different muscles and in different fiber types within a muscle. The width is related to the number of zigzag bands or chevrons seen in longitudinal sections. Rowe (1973) showed that in rat plantaris muscle, the white, intermediate, and red fibers have Z-bands, which comprise, respectively two, three, and four chevrons with a periodicity parallel to the fiber axis of ~40 nm. There are two basic types of muscle in fish. Red slow muscle is contained in a thin strip along the lateral line; it is responsible for gentle swimming in the fish (Rome et al., 1988). This muscle has a moderately wide (~100 nm) Z-band (Munro, 1986). The bulk of the fish is formed by fast white muscle, which is used for rapid energetic swimming (Rome et al., 1988). The Z-band in fish white muscle, the subject here, is narrow with a single zigzag structure and very little overlap of oppositely oriented actin filaments (Fig. 1 *a*; Franzini-Armstrong, 1973). Termed the "simple" Z-band, it is therefore important as it represents the most fundamental Z-band organisation.

Previous models of the vertebrate Z-band were constructed to account for individual electron microscope views of longitudinal (LS) and transverse sections (TS) (e.g., Knappeis and Carlsen, 1962; Yamaguchi et al., 1985). In the former case the appearance is often that of a zigzag-shaped linking structure (Fig. 1 *a*) connecting the ends of actin fila-

1. *Abbreviations used in this paper*: LS, longitudinal section; 3D, three dimensional; TS, transverse section.

ments offset by half a period on each side of the Z-band. In transverse view, the actin filament lattice on either side of the Z-band is tetragonal with a period ranging from 19 to 25 nm, the lattice on one side relative to the other side similarly being offset by half a period along the orthogonal axes. In this view there are two typical appearances, shown diagrammatically in Fig. 1, *b* and *c*, the so-called small-square lattice and the basketweave appearance. Combining the basketweave appearance with the zigzag view in LS, led Knappeis and Carlsen (1962) to propose a model of the Z-band in which there are four links from the end of one actin filament to the ends of the four actin filaments in the opposite sarcomere. Since the small-square and basketweave appearances often appear within the same myofibril, researchers have particularly endeavored to produce Z-band schemes that allow transition between the two forms (Macdonald and Engel, 1971; Yamaguchi et al., 1985; Goldstein et al., 1979, 1982, 1987). These authors have suggested that the transition from one form to the other could occur after a change in the curvature of the links. For example, the basketweave form could be transformed into the small-square form by tighter curvature of the links (labeled *ss* in Fig. 1 *c*). The Z-band of fish white muscle described here has an appearance in transverse sections unlike both the typical basketweave and small-square lattice views but it will be shown that the links follow a basketweave course.

Any model of the Z-band must comply to some degree with the symmetry of the underlying actin filaments. A vertebrate actin filament has approximate helical symmetry of 13 G-actin subunits in six turns in an axial repeat of ~73 nm (Huxley and Brown, 1967). Equivalent points on the surface of the actin filament are therefore repeated 167° round (anticlockwise) and 2.73 nm along the filament. Hence the double-stranded appearance of an actin filament gives approximate twofold symmetry when viewed at low resolution. On the grounds of actin filament symmetry alone, the Knappeis and Carlsen model is not tenable, since it requires four identical and rotationally symmetric links between opposing actin filament arrays. An implicit assumption in the Knappeis and Carlsen model is that the zigzag appearance seen in LS occurs along both the principal projections of the tetragonal lattice. It will be shown here that this assumption is incorrect since the views, termed here the [10] and [01] views, are quite distinct; only one of them, the [10] has the zigzag view.

The 3D reconstruction of the Z-band in fish white muscle is described here. Although the structure will be shown to have approximate twofold symmetry normal to the plane, the true symmetry appears to be best described by the two-sided plane group $p12_1$ (using the terminology followed in Amos et al., 1982) with the screw axis in the plane. Some of the results discussed here have been presented as conference proceedings previously (Luther, P. K., and M. Squire, 1985. *J. Muscle Res. Cell. Motil.* 6:77; Luther, 1989).

Materials and Methods

Sample Preparation

A freshly killed fish (roach, *Rutilus rutilus*) was skinned and the body muscle in the relaxed state was fixed in situ in 2.5% glutaraldehyde in phosphate buffer. Small strips of white body muscle were then fixed in 1% osmium tetroxide, dehydrated in an ethanol series and embedded in Araldite. The

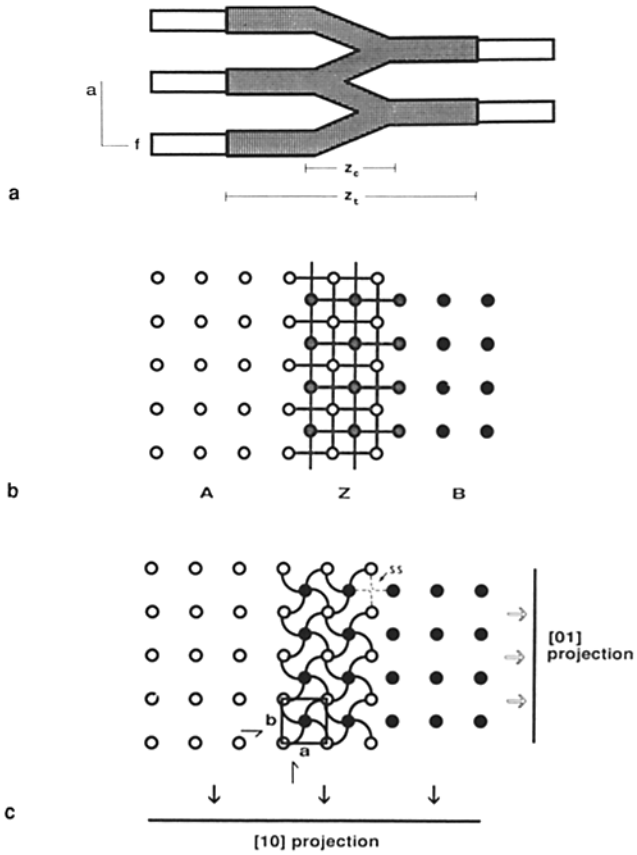

Figure 1. Schematic representations of the characteristic views of vertebrate Z-bands as seen in longitudinal sections (*a*) and in transverse sections (*b* and *c*). The lattice spacing varies from 19 to 25 nm. (*a*) The Z-band in fish white muscle shows a single zig-zag appearance with higher density (*shaded*) compared with the density of the nearby actin filaments (*unshaded*). The total width of the Z-band (Z_t) is 70–90 nm and the width of the central part (Z_c) is ~15–25 nm. The *a* cell axis is shown; *f* represents the actin filament direction. In the transverse views, *b* and *c*, actin filaments from adjacent sarcomeres are represented by open circles (*A*) and filled circles (*B*), respectively. The so-called small-square form in *b* shows apparent direct connections between filaments of the same polarity. The basketweave form, *c*, shows apparent direct links between filaments of opposite polarity in facing sarcomeres. Researchers have proposed that transformation of one form to the other can be achieved by varying the curvature of the links e.g., the basketweave form can be transformed to the small-square form by tighter curvature of the links as shown by the dashed lines labeled *ss* in *c* (Yamaguchi et al., 1985; Goldstein et al., 1979, 1982, 1987). The nomenclature followed in this work is illustrated in *c*.

For one unit cell, the *a*- and *b*-axes are labeled. Longitudinal sections cut parallel to the *a*-axis produce the [10] projection or view and longitudinal sections cut parallel to the *b*-axis produce the [01] projection. It will be shown that only the [10] view has the zigzag appearance. The symmetry elements relevant for this work are shown. For the unit cell drawn, with twofold screw axes parallel to the *a*- and *b*-axes in the central plane of the Z-band, along with twofold rotational symmetry along the actin filaments, the symmetry is described by the two-sided plane group $p22_12_1$ (as described in Amos et al., 1982). If the only symmetry element is a twofold screw axis e.g., parallel to the *b* axis as found here, then the overall symmetry is $p12_1$.

cured block was subjected to 2 min microwave radiation in a domestic microwave oven, as this treatment is thought to produce more stable sections for EM (Kinnamon, 1989). Thin silver-coloured sections were cut on a Huxley Mark II ultramicrotome and stained with 2% uranyl acetate followed by Reynolds lead citrate.

Electron Microscopy

The sections were examined in a JEOL 1200EX electron microscope fitted with a rotation goniometer. For the 3D reconstruction, survey micrographs of transverse sections of potential areas were first obtained and the best regions of Z-band were selected by optical diffraction. The chosen area was viewed at 30,000 times magnification and electron micrographs recorded for two tilt series about mutually perpendicular axes in steps of 5° from −60° to +60° about one axis and from −60° to +40° about the other. Longitudinal sections were also used to view the appearance of the Z-band about the [10] and [01] projections. For this the sections were tilted about the myofibril axis until either of these views was seen. Then a few micrographs were recorded on either side of this angle in steps of 2–4°. The clearest views were selected later. Whenever possible the section was tilted to view down the complementary lattice projection (the [10] or [01]) and new images recorded.

Determination of Section Thickness

Knowledge of the section thickness determined independently of the 3D reconstruction is useful, since it allows better comparison of features in the 3D map with features of previously known size in the electron microscope. The approximate section thickness can be judged from the interference color when cutting the section. More quantitative estimates were obtained by applying gold particles to each side of the section and then viewing the particles at various tilt angles (method of Luther et al., 1988). Two different areas of gold particles were examined on the section used for the 3D reconstruction and the program ALIGN written by M. L. Lawrence (CSIRO, Parkville, Victoria, Australia) was used to compute the section thickness (Luther et al., 1988). For minimal-dose microscopy, as used in this work, collapse of the section to 70% of the original thickness occurs in the microscope (Luther et al., 1988) and this correction was applied to determine the thickness of the native material.

Image Processing

The micrographs were scanned on a Joyce-Loebl Scandig (Gateshead, UK) microdensitometer with a step size of 25 μm. In the case of longitudinal sections, the images of the Z-bands were enhanced by Fourier filtering. For this the Fourier transforms were filtered by selecting three thin strips parallel to the equator and located on the equator, the 10 (or 01) and the 20 (or 02) diffraction spots. The 3D reconstruction was done from a transverse section of the Z-band after the general methods described by Amos et al. (1982). For the image processing, software written at the Cambridge MRC Laboratory of Molecular Biology was used for Fourier transformation, merging of the data and inverse transformation. Software written inhouse was used for viewing the images and the transforms and for obtaining hardcopies on a Postscript laser printer or Hewlett-Packard Laserjet laser printer. The 3D reconstructions were viewed on an Evans and Sutherland PS300 imaging system running Frodo.

Simple 3D computer models to interpret the reconstruction of the fish Z-band were constructed using the software DesignCAD 3-D (American Small Business Computers, Pryor, OK) running on an IBM-AT compatible computer fitted with a VGA card and a Zenith ZCM-1490 flat-screen monitor.

Results

Analysis of Longitudinal Sections

Fig. 2, *a* and *b* shows electron micrographs of the Z-band in fish white muscle in a longitudinal section tilted about the myofibril axis for the [10] and [01] views of the actin filament lattice. The two views are quite distinct. To visualize the appearances more clearly, the boxed areas in *a* and *b* (enlarged in the insets) were Fourier filtered and the resulting images are shown in Fig. 2, *c* and *d*, respectively. The views are depicted schematically in Fig. 2, *g* and *h*. Only the [10] view in Fig. 2, *a* and *c* has the zigzag appearance comparable to the schematic diagram in Fig. 1 *a*. The [01] view looks very different: it appears like a lattice of interdigitating spikes. Lack of density in the region between any two opposing actin filaments (*arrows*, Fig. 2 *d*) does not necessarily mean lack of linking structure, but that in this projection the density attributable to the spike shapes is relatively much greater than in the gap regions. The high density region in the middle of the Z-band (labeled Z_c in Fig. 2 *c*) has a width ranging from 15 to 25 nm. As will be shown from the 3D reconstruction, the high-density region can be attributed to the overlap of the actin filament ends as well as cross-linking material. The total axial width of the Z-band (Z_t in Fig. 1 *a*), indicated by the thickened regions of the actin filaments enclosed within the widths of the boxed regions in Fig. 2, *a* and *b*, varies from 70 to 90 nm in this muscle. The thickened region sometimes appears smaller in the [01] view as in Fig. 2 *b*.

The lattice spacing measured from several longitudinal sections of this preparation was 21.1 ± 2.7 nm (n = 15). In each case the measurement was done relative to the A-band cross-bridge periodicity of 43 nm. For the purpose of discussion in this paper, a standard value of 21 nm is used for the lattice spacing.

3D Reconstruction

The reconstruction was done from a transverse section of the Z-band as shown in Fig. 3 *a*. As mentioned above, the appearance of the fish white muscle Z-band is unlike both the basketweave and the small-square lattice. The thickness of the section was determined in two different regions. The values obtained were 43 and 37 nm. Assuming shrinkage to 70% of the starting value for the minimal dose EM used (Luther et al., 1988) the original mean thickness is ~48 nm. Such a thickness ensures that all of the central high density region of the Z-band (Z_c in Fig. 1 *a*) and a large part of the thickened actin shaft area on each side is included for the 3D reconstruction. The rectangular boxed region in Fig. 3 *a* was used for the reconstruction. The computed diffraction pattern is shown in Fig. 3 *b* and the 10 and 02 spots are indexed. The transform spots seen are of types 10, 11, 20, and 21 with occasional signs of 22. Searching the diffraction pattern for symmetry, the absence of the 01 spot suggests glide plane symmetry in this projection with the axis parallel to the *b*-axis. Analysis of the phases of the spots also favored a glide plane along the same direction. Some departure from this symmetry is indicated by the asymmetry of the amplitudes of the 11 and −11 spots. Glide plane symmetry in projection corresponds to twofold screw symmetry in the 3D structure.

Tilt views of the boxed region in Fig. 3 *a* were recorded in steps of 5° about two orthogonal axes. Since the period is taken to be 21 nm, this means that the resolution in the reconstruction is ~10 nm in the plane of the Z-band. The resolution perpendicular to this plane can be judged from the profiles of the low order spots, the 10 and 01, which extend to $z^* = 0.08$ nm^{-1}, i.e., the resolution is 12.5 nm. For the untilted image, P2 symmetry was assumed only to locate the best twofold origin in the unit cell. The transform data were merged assuming P1 symmetry. The data merged with low-phase residual, <20°, but in a few cases phase residuals up

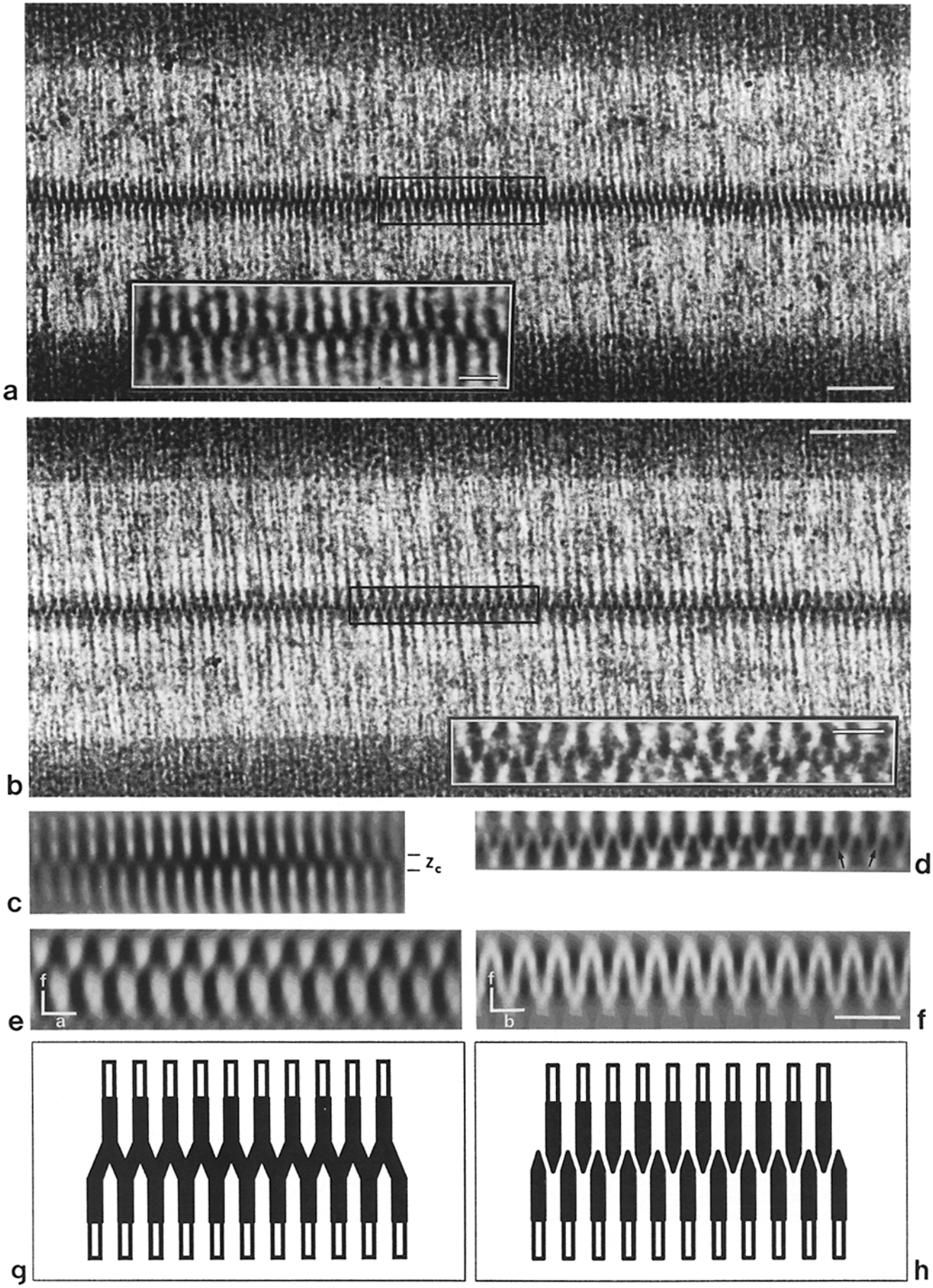
a
b
c
z_c
d
e
f
a
f
b
f
g
h

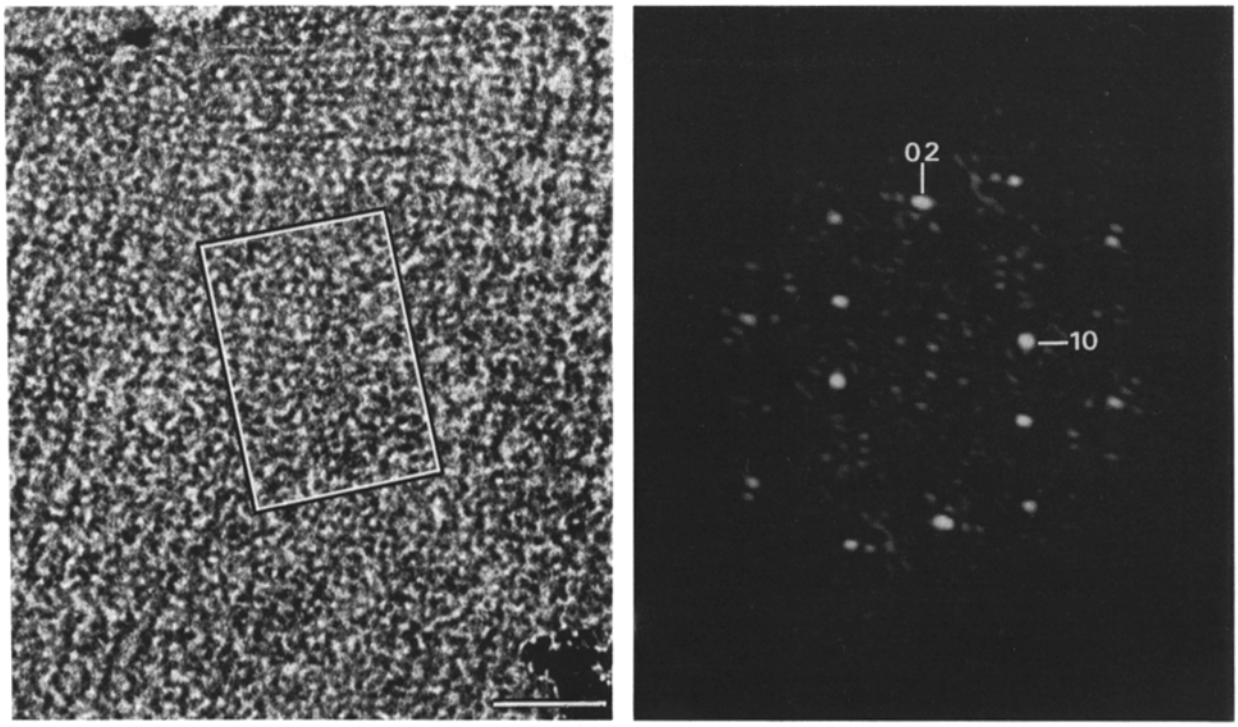

Figure 3. (*a*) Transverse section of roach (*Rutilus rutilus*) white body muscle showing the Z-band region (boxed) used for 3D reconstruction. The thickness of the section, determined by labeling the section surface with gold particles (method of Luther et al., 1988), is ~48 nm before the EM (details in text). For the 3D reconstruction, images were obtained by tilting the section in steps of 5° about axes parallel to the sides of the boxed region. The tilt range about one axis was −60° to +60° and about the other was −60° to +40°. (*b*) Computed diffraction pattern of the boxed region in *a*. The indexing scheme is marked. The systematic absence of the 01 diffraction spot indicates screw symmetry present in the 3D structure. Bar, 100 nm.

to 40° occurred. Fourier transform profiles for the prominent lattice lines are shown in Fig. 4. The 3D transform lacks information along the 00*z** lattice line. This information affects the mean density of the sections calculated along *z* in the reconstruction. It can be obtained from the Fourier transform of a longitudinal section or in real space from the projection of a longitudinal section of the Z-band normal to the myofibril axis. However inclusion of the LS data made little difference to the features seen and so they are excluded from the reconstruction described here. The Fourier transform of an [01] longitudinal section was used to extend the 01 lattice line which was incomplete because of limited tilt of 40° in one direction.

The 3D reconstruction of the fish Z-band is first compared with the appearance seen in the longitudinal section illustrated in Fig. 2. For this the reconstruction was projected along the appropriate directions to show the [10] and [01] views and the resulting images are shown in Fig. 2, *e* and *f*. The projections are very similar in appearance to the filtered LS views in Fig. 2, *c* and *d*. The [10] projection of the reconstruction *e* shows a zigzag pattern similar to the LS in *c*. The [01] projection in *f* shows the interdigitating spike pattern similar to the LS view in *d*.

Comparison of the [10] projection in *e* with the LS view, *c*, allows us to define the region being reconstructed in relation to the Z-band. It is clear that the whole of the high den-

Figure 2. Analysis of longitudinal sections of fish muscle Z-band. The section was tilted about the myofibril axis to view clearly (*a*) the [10] and (*b*) the [01] projections of the thin filament lattice. The [10] view shows the characteristic zigzag appearance; a clear example is boxed and shown enlarged in the inset and in the Fourier filtered image (*c*). For the [01] view a region is also boxed, enlarged in the inset and the filtered image shown in *d*. In this case the appearance is that of a lattice of overlapping spikes. Shown below each filtered view is the corresponding projection (*e* and *f*) of the 3D reconstruction of the fish Z-band (see later). The [10] projection (*e*) shows a clear zig-zag. The [01] view (*f*) of the reconstruction also shows a set of overlapping spikes. The two views are depicted schematically in Fig. 2, *g* and *h*.

The total axial width of the Z-band (Z_t in Fig. 1 *a*) is reckoned from the thickened stems of the actin filaments enclosed within the boxed regions in *a* and *b* and this is 70–90 nm. The axial width of the central high density region in *c* (Z_c in Fig. 1 *a*) is 15–25 nm. Note that the images shown in *a* and *b* are of different Z-bands (in fact they were located on two sides of a sarcomere). They were chosen as particularly clear examples of the relevant views. The author has several examples of Z-bands that when tilted at suitable angles about the myofibril axis, show both the [10] and the [01] views, which are very similar to those shown here. High protein density is black. The *a* and *b* cell axes are marked in *e* and *f*, respectively. *f* represents the actin filament direction. Bars: (*a* and *b*) 200 nm; (*a*, *inset* and *c*) 50 nm; (*b*, *inset* and *d*) 50 nm; (*e* and *f*) 50 nm.

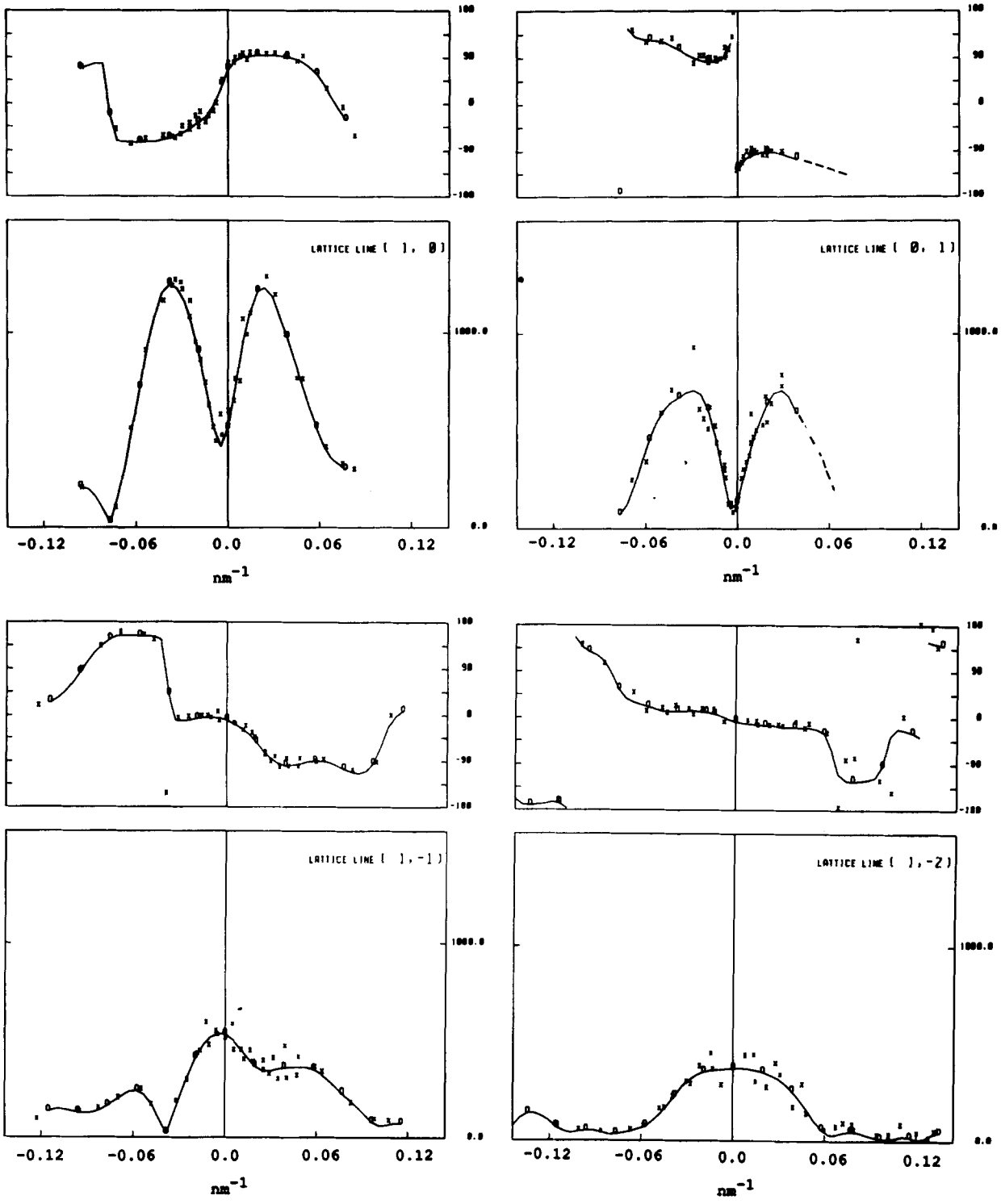

Figure 4. Variation of amplitude (*bottom*) and phase (*top*) along z^* for four prominent Fourier spots. The plots were obtained assuming minimal P1 symmetry. The crosses (X) represent experimental data, the circles (o) represent the sampled values used for the reconstruction. The 01 lattice line data was incomplete because the section could only be tilted to 40° in one direction. By comparing with the Fourier transform of a longitudinal section, two more points were added to the 01 data at $z^* = 0.06$ and 0.08 nm^{-1}. As shown by the dashed lines, this made the graph symmetrical about the y-axis.

sity central part (Z_c in *c*) is included in the reconstruction. The projection also shows that the center of the Z-band in the reconstruction is located just above the middle of the section thickness. When the 3D model was viewed it showed that the majority of the crosslinking material occurred in the middle 30 nm of the reconstructed thickness. Outside of this region on each side there were fairly constant actin filament profiles.

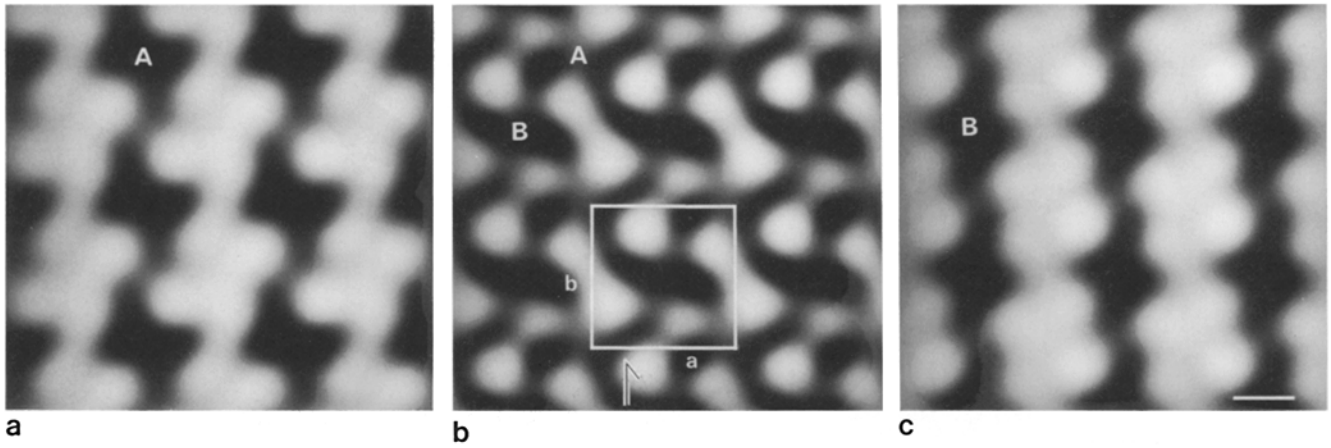

Figure 5. Z-band 3D reconstruction. Three sections, three by three unit cells wide, represented in tonal form (high protein density depicted by dark shading) showing the middle (*b*) of the Z-band and regions *a* and *c* ~12 nm to each side of the center. High density occurs at the actin filament positions; in *a*, an example is marked *A*; in *c*, which represents actin filaments with opposite polarity, an example is marked *B*. One unit cell with the *a*- and *b*-axes marked is shown in *b*. The terminal regions of the actin filaments overlap in the middle as seen in the central section *b* and there are links (Z-links) between filaments of opposite polarity. A new Z-band feature seen in the outer regions *a* and *c* is the presence of links (polar links) between filaments of the same polarity. In each case the polar links run parallel to the *b*-axis. The central section (*b*) shows an approximate glide plane symmetry parallel to the *b*-axis. In 3D this corresponds to a twofold screw axis which relates one half of the Z-band to the other. *a* and *c* are thus related. Bar, 10 nm.

Fig. 5 shows three sections of the 3D reconstruction, with density depicted as shades of grey (*black* is protein). Fig. 5 *b* depicts what is believed to be the view of the central plane of the Z-band. This was selected by searching in the 3D density map for the section which contained the best 2_1 screw axis. The sections shown in Fig. 5, *a* and *c* are located about 12 nm on each side of the central plane in Fig. 5 *b*. Two actin filaments from the adjacent sarcomeres are labeled A and B, respectively in Fig. 5, *a* and *c*. They amply illustrate the basic features of the Z-band: strong actin filament profiles, with half unit cell displacement relative to the lattice in the adjacent sarcomere. Crosslinking structure between the oppositely oriented actin filaments is seen in the central section in *b*. These links will be referred to as the Z-links. A new feature of actin linkages in the Z-band is seen in *a* and *c*: these figures show there is linking material between actin filaments of the same polarity and in each case this runs in the same direction, parallel to the *b*-axis. These links will be referred to as polar links.

The density maps in Fig. 5, *a–c* show approximate twofold rotational symmetry centered on an actin filament. There also appear to be two approximate twofold screw axes which for example, relate to Fig. 5, *a* and *c*, located in the central plane of the Z-band. The more prominent screw axis parallel to the *b*-axis is marked.

Part of the 3D reconstruction is shown as a stereo view in Fig. 6 *a*. The structure is bounded by a density contour selected to optimize the view of actin filament profiles and the cross-links. The stereo view includes a slab of depth 25 nm from the whole 50 nm reconstruction. The slab thickness was chosen to show fully the structure of the interior comprising the Z-links and to show in part the polar binding region between actin filaments of the same polarity. The ends of two actin filaments of opposite orientation are labeled A and B. The stereo view shows four Z-links connecting each actin filament to the facing four antipolar actin filaments. The links are labeled C1 to C4 in the figure. At either end a link appears to join the actin filaments at a grazing angle and continues along the filament for ~10–15 nm. Links C1 and C2 emanate from nearly diametrically opposed locations near the end of the actin filament B (proximal sites) and attach across to the stems of two A actin filaments at sites 5–10 nm from the filament tip (distal sites). Links C3 and C4 located ~80° round from C2 and C1 behave in the opposite fashion: they are attached to the distal sites of B filament stems and link across to the proximal sites of the A filaments. Link C4 appears weaker than the other three links. The reconstruction shows that the terminal regions of the oppositely oriented actin filaments overlap in the middle of the Z-band by ~10 nm.

Located 10–15 nm from the middle there are links between actin filaments of the same polarity. Links P_A join the A filaments and links P_B join the B filaments. These polar links run in the same direction (parallel to the *b*-axis). In this reconstruction, the P_B links appear slightly stronger than the P_A links: in the native muscle they are probably of similar densities. There appears to be some continuity of density between the distal sites and the polar links.

For the stereo view in Fig. 6 *b*, lines were drawn to run as closely as possible through the centers of the Z-links to demonstrate their course in 3D. In Fig. 6 *c*, only these central lines through the Z-links are shown in 3D. Stripped of their bulk, it is clear from Fig. 6 *c* that the Z-links follow a basket-weave pattern.

In the stereo view of the reconstruction in Fig. 6 *a*, there appear to be approximate twofold rotation axes along the actin filaments, and two 2_1 screw axes located in the central plane of the Z-band running parallel to the *a*- and *b*-axes. The more prominent screw axis parallel to the *b*-axis is marked.

To show more clearly the relation between the Z-links labeled C1 to C4 in Fig. 6 *a*, the actin filaments marked A and

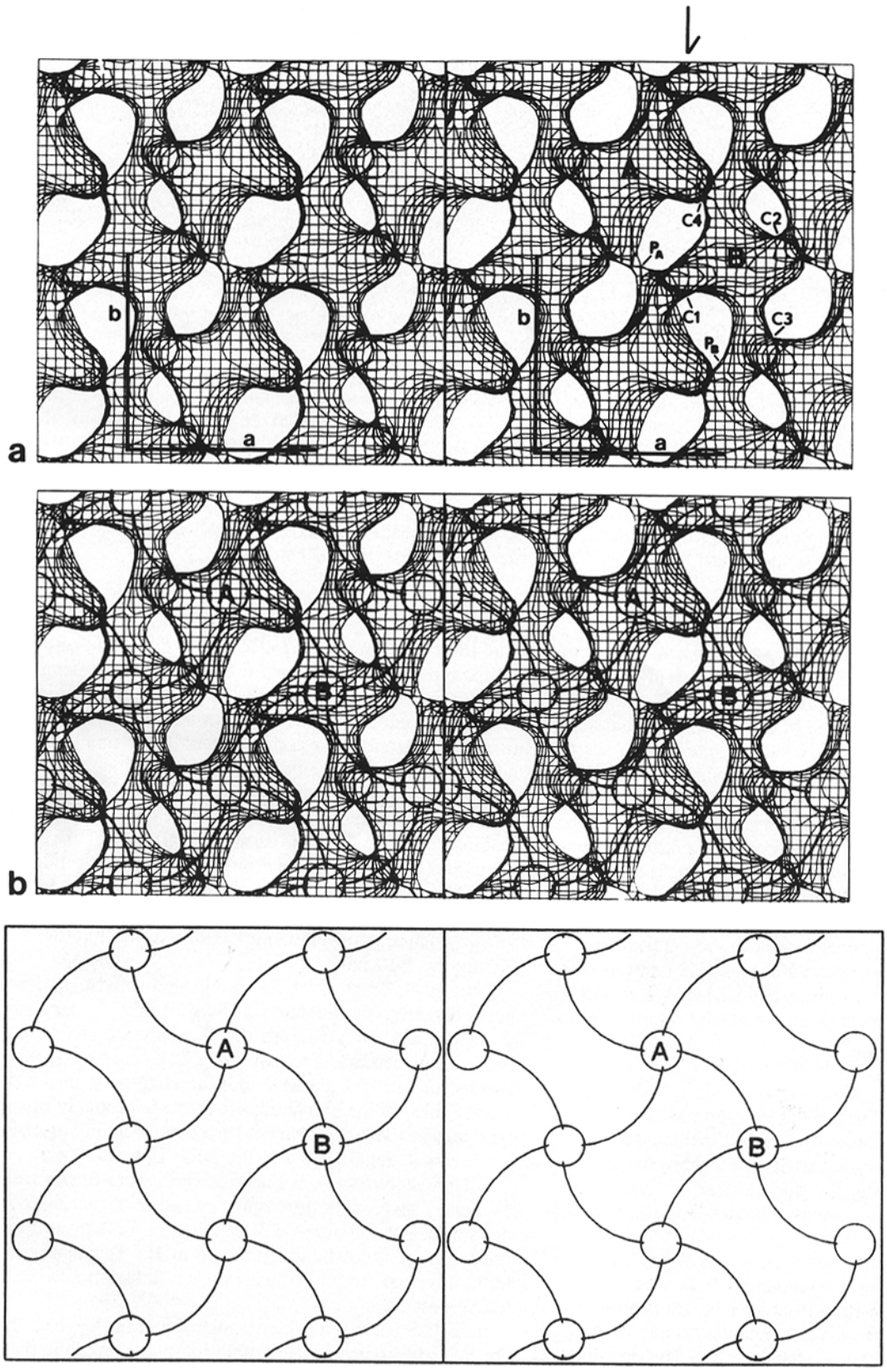

Figure 6. (*a*) Stereo image of part of the Z-band 3D reconstruction viewed down the actin filament axis. The image was obtained on an Evans and Sutherland PS300 computer by selecting a region ~25 nm deep. The terminal ends of actin filaments from the adjacent sarcomeres are seen and examples are labeled A and B. In the interior 10 nm there are links, the Z-links, labeled C1 to C4 between the opposite polarity actin filaments. In relation to filament B, links C1 and C2 originate near the end of the filament (proximal site) from the left and right sides as illustrated. These links attach at a grazing angle to the reverse polarity filaments at sites ~5–10 nm further from the end (distal sites) and these sites are located at the top and bottom of an actin filament as illustrated. Links C3 and C4 have distal attachment

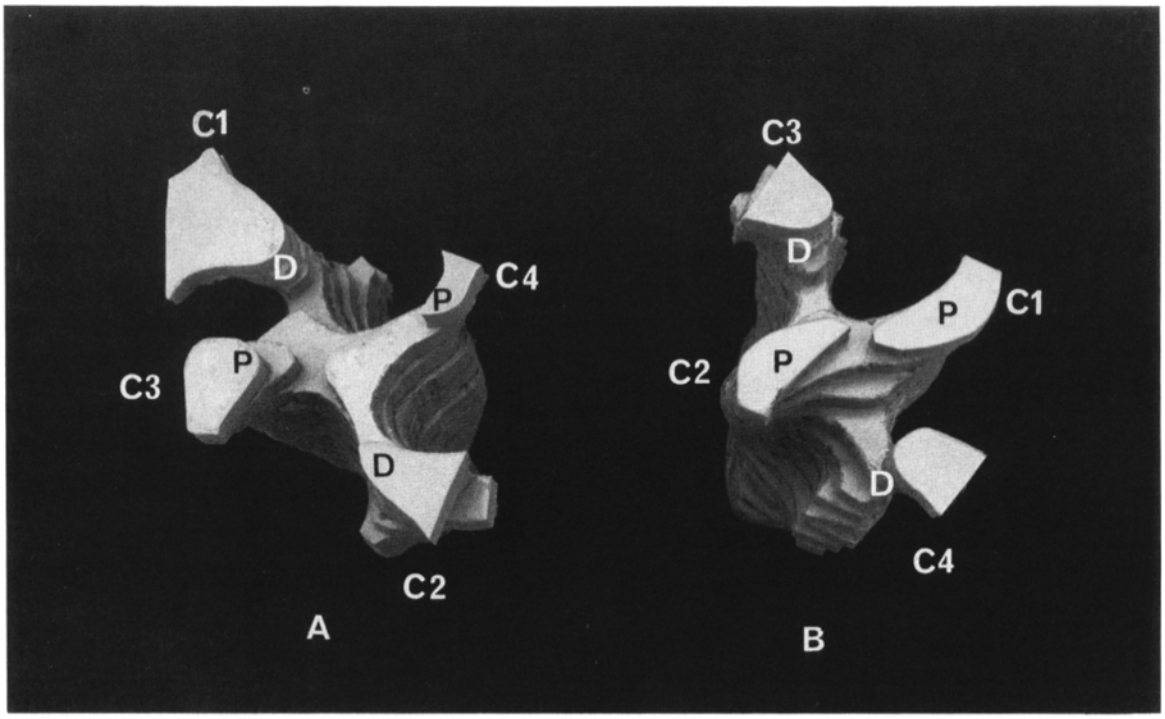

Figure 7. Photograph of solid models of the 3D reconstruction showing an actin filament A, and the reverse polarity filament B, together with the associated links. The arrangement of the proximal (P) and distal (D) sites is seen clearly. See text for full description.

B were cut out from the 3D map along with parts of the link domains and solid models built using 5-mm modeling board. Fig. 7 shows the A filament upright and the B filament inverted with all the relevant links labelled. The distal domains (*D*) are very similar in A and B and also the proximal domains (*P*) are very similar. The distal domains appear to run along the shaft for ~15 nm, compared with ~10 nm for the proximal domains. There is approximate twofold rotational symmetry along each actin filament. If the course of the links is followed, it is noted that there is reversal between distal and proximal attachment between the A and B filaments e.g., the distal domain of C1 located on A attaches as a proximal domain on filament B.

Modeling the Fish Muscle Simple Z-band

To understand the difference in the longitudinal [10] and [01] views, a simple model with twofold rotational symmetry was constructed as shown in Fig. 8. The basic building unit for the [10] zigzag view is illustrated in Fig. 8 *a*. A 25-nm long, 10-μm-diam actin filament is represented by the lightly shaded cylinder. A complete Z-link that connects two oppositely oriented filaments is modeled as a cylindrical tube of diameter 5 nm comprising three domains: a proximal (P) domain of length 10 nm along one actin filament which runs up to the filament tip; a spanning (S) domain 7 nm long which spans the diagonal of the actin lattice towards the oppositely oriented filament and a 15-nm-long distal (D) domain located along the opposite polarity filament starting 5 nm from the filament end. In Fig. 8 *a*, a distal domain is shown attached along the front of an actin filament and the proximal domains are attached at the sides. The spanning domains which run along the diagonals are shown foreshortened. Fig. 8 *a* represents the basic unit for the [10] view. Rotating the basic unit by 90° along the filament axis produces the basic unit for the [01] view as shown in *b*. Composite views of the [10] and [01] projections can be produced by placing the basic units on lattices of spacing 21 nm and then docking inverted copies to make contact between the spanning domains. The resulting composite [10] and [01] views are shown in Fig. 8, *c* and *d*, respectively. Fig. 8 *c* shows that in the [10] view considerable density builds up along a zigzag. From Fig. 8 *d* we can understand that the [01]

sites on B and proximal sites on the A type filaments. There are also links, the polar links, between similar polarity filaments labeled P_A for the A set and P_B for the B set. The P_B links appear denser than the P_A links. Note that the polar links run nearly parallel to the *b* cell axes. In the stereo view (*a*), there appear to be approximate twofold rotation axes along the actin filaments, and two 2_1 screw axes located in the central plane of the Z-band running parallel to the *a*- and *b*-axes. The more prominent screw axis parallel to the *b*-axis is marked. (*b*) Stereo image of (*a*), illustrating the course of the Z-links. Lines have been drawn to run through the middle of the Z-links. The fit is approximate, since each line follows an arc that passes through only three points measured from the reconstruction along each of the four unique Z-links. The circles are placed at the best judged centers of the actin filaments in the central plane of the Z-band. (*c*) Stereo image derived from *b* showing only the course of the Z-links in 3D. Again the circles represent actin filament centres in the central plane of the Z-band. As in *a* and *b*, the actin filament labeled A enters from below the plane of the page and the filament B enters from above the plane. Stripped of the bulk of the Z-links, this figure shows that the Z-links follow a basketweave course.

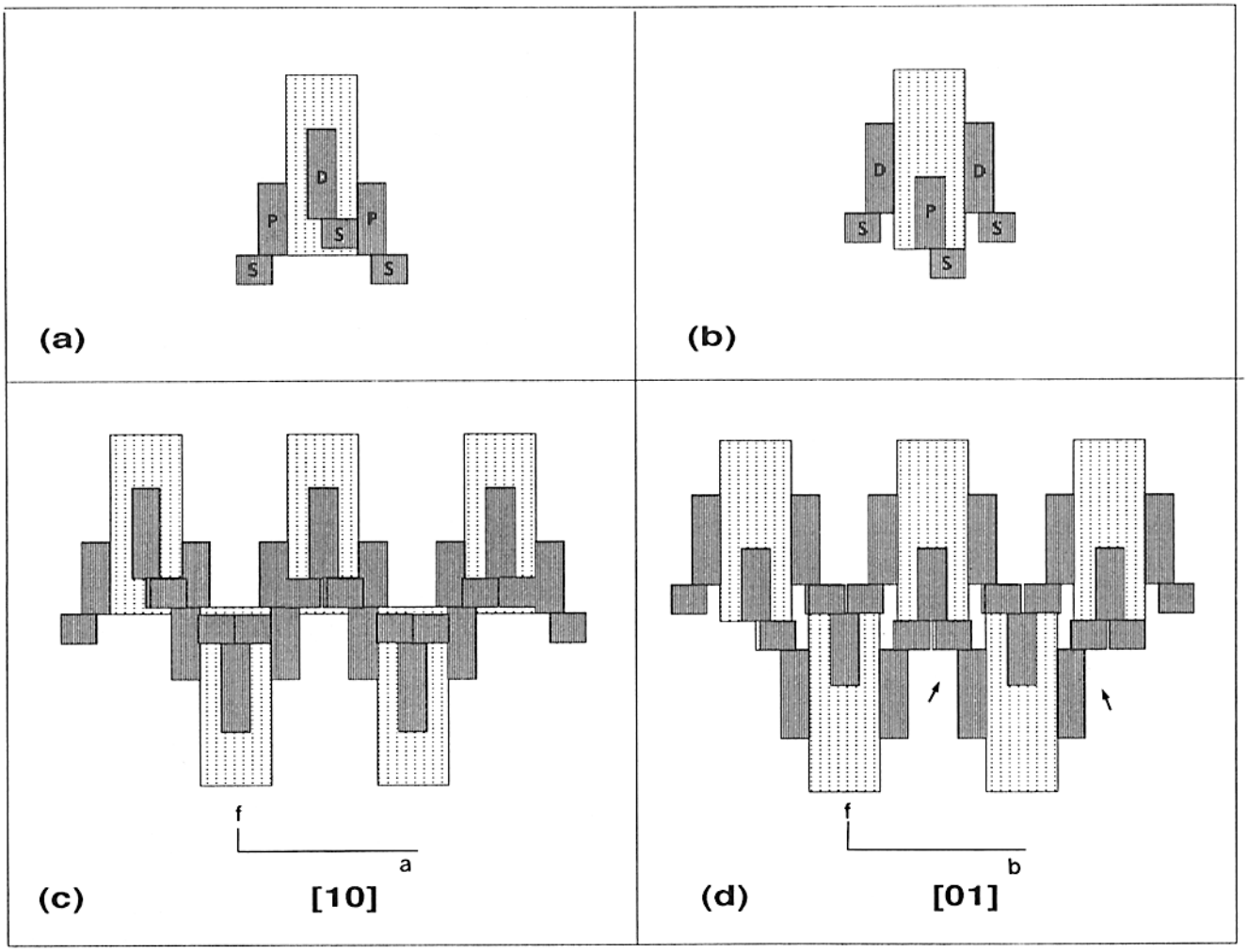

Figure 8. Modeling the [10] and [01] views of the fish Z-band. *a* and *b* represent the repeating units for the [10] and [01] views respectively for a simple twofold model of the Z-band (overall symmetry is therefore $p22_12_1$). Twofold symmetry has been assumed to ease construction of the model. The lightly shaded boxes represent actin filaments; the dark shaded boxes represent link domains: *P*, proximal; *S*, spanning; *D*, distal. Proximal domains are located near the actin filament tip and the distal domains are located about 5 nm further from the tip. The [01] view in *b* is obtained by rotating the [10] model in *a* by 90°. The composite models in *c* and *d* were obtained by placing upright copies of the respective units on a lattice of 21-nm spacing and then docking inverted copies to match the spanning links. The composite [10] view in *c* has considerable density labeling a zigzag appearance. The [01] view in *d* shows gaps in the Z-band along the arrowed regions: the effect of this in projection would be to emphasize the spiked rods appearance as observed in longitudinal sections. The *a* and *b* cell axes are shown and *f* represents the actin filament direction.

appearance of overlapping-spikes is due to the density derived from the proximal domains attached at the tip. As in the Z-band longitudinal section in Fig. 2 *d* and in the reconstruction in Fig. 2 *f*, there is weakness of density along the arrowed regions.

The simple twofold model of the fish Z-band described above was constructed as a solid model by computer, and surface views are shown in Fig. 9. The plan view is shown in *a* and all the links are labeled in *b*. A stereo view of the model is shown in *c*. The white circles in *a* and the grey cylinders in *b* and *c* represent actin filaments. Z-links related by twofold symmetry around each actin filament are shown in the same color (purple or yellow); the links of one color are related to the links of the other color by 2_1 screw axes in the plane of the Z-band. The polar links shown in green run parallel to the *b* axis.

Discussion

Symmetry and Past Models

This study has shown that the Z-band in fish white muscle, termed "simple" by Franzini-Armstrong (1973), lives up to this description when analyzed fully in 3D. The main features of the Z-band are observed in the reconstruction: shafts of actin filaments from adjacent sarcomeres are based on a tetragonal lattice with relative half unit cell displacement and the [10] projection of the 3D map shows the single zigzag appearance commonly seen in longitudinal sections. Described here for the first time are the details of the [01] view, shown to be distinct from the [10] zigzag view, comprising a lattice of interdigitating spikes overlapping by ~10 nm.

Each Z-link between a pair of oppositely oriented actin

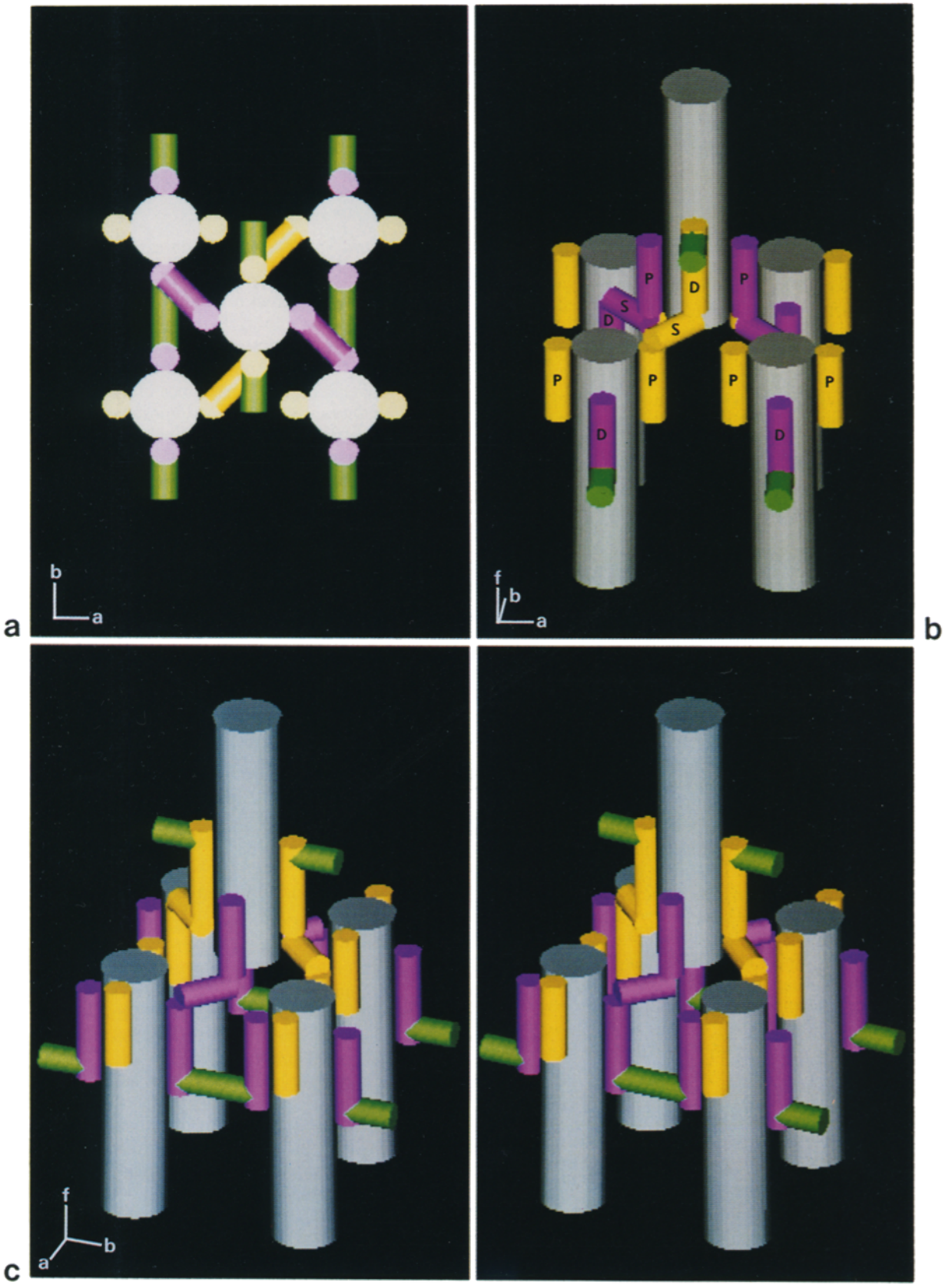

Figure 9. Surface representation of the basic Z-band model of Fig. 8 showing the course of the links. Although the fish Z-band has only approximate twofold symmetry centered on an actin filament, this symmetry has been incorporated here to aid construction of the model. Z-links related by twofold symmetry are shown in the same color (*purple* or *yellow*). Polar links, running parallel to the *b* axis, are shown in green. (*a*) Plan view. As in the side views illustrated in *b* and *c*, the central actin filament (*white*) is above the four surrounding filaments from the adjacent sarcomere. (*b*) View of the model with all the Z-link domains labeled: *P*, proximal; *S*, spanning; *D*, distal. (*c*) Stereo view of the model. In each figure, the *a* and *b* cell axes are labeled and *f* represents the actin filament direction.

filaments from adjacent sarcomeres appears to consist of three domains: a proximal domain along the actin filament of length ~10–15 nm starting from the filament tip, a spanning domain joining the two filaments and finally along the opposite filament, a distal domain running from 5 to 10 nm from the filament tip for a length of ~15–20 nm. The agreement between the modelling studies and the appearance in longitudinal sections and projected views of the 3D reconstruction confirms the validity of this interpretation.

The original model for the simple Z-band proposed by Knappeis and Carlsen (1962) was correct in requiring four links between one actin filament and the facing four oppositely directed filaments from the adjacent sarcomere, but was incorrect regarding symmetry, since the links in their model were identical and placed with fourfold symmetry. In this work, the following approximate symmetry relationships have been found in the Z-band. In the plane of the Z-band there are two twofold screw axes that run parallel to the *a*- and *b*-axes. Normal to the plane there is a twofold rotation axis centered on the actin filaments. The approximate overall symmetry is therefore described by the two-sided plane group $p22_12_1$. The models described in Figs. 8 and 9 were based on this symmetry for ease of construction. That this symmetry is only approximate and not the true symmetry is based on the following. Actin filaments do not have twofold symmetry as mentioned earlier (Huxley and Brown, 1967). Analysis of the phases in the Fourier transform of the untilted image gave better support for a glide plane parallel to the *b*-axis than the *a*-axis. Further evidence for the glide plane parallel to the *b*-axis was obtained from examining the amplitudes of the same transform, which showed the systematic absence of the 01 spot. The symmetry of the Z-band therefore is very likely described by the two sided plane-group $p12_1$ with the screw axis parallel to the *b*-axis.

In the reconstruction, each member of a pair of distal domains around an actin filament appears to be at the same height along the filament. Similarly each proximal link member around an actin filament appears to be at the same height along the filament (but different from the height for the distal links). It is probable that in the native structure there may be a 2.7-μm shift between the two proximal or the two distal domains as expected from the actin filament symmetry. However, such a shift could not be seen at the resolution of the current reconstruction. It is easier to measure the approximate axial shift between the two types of link (proximal and distal) and this is ~5–10 nm. Since there is a rotation of 80° between the two types of link, in the native structure the axial shift may be expected to be 15–20 nm. The disparity may be due to the lack of resolution axially or may be caused by changes in the actin filament twist as reported before (Egelman et al., 1982). The handedness noted for the Z-band has the form of a right-handed twist of the linking elements attached to the actin. This may correspond to the right handed long pitch helix of the actin filament.

Polar Links

A novel feature of the observed Z-band linkages are the polar links which connect actin filaments of the same polarity in a direction parallel to the *b*-axis. These links are located about 10–15 nm on each side of the Z-band center.

In the reconstruction the polar links are the main structural features located outside the central Z-link region. In longitudinal sections, the location of the polar links must be at the thickened actin filament stems such as those observed within the boxed regions in Fig. 2, *a* and *b* and shown schematically in Fig. 1 *a*. Such thickened actin stems are also seen in the peripheral regions of Z-bands from many vertebrate muscles irrespective of the Z-band width (Goll et al., 1969; Franzini-Armstrong, 1973; Goldstein et al., 1979). It is probable that these thickened stem regions in other muscles represent similar polar link regions.

Basketweave and Small-Square Z-bands

As mentioned before, the appearance of the roach Z-band in transverse sections is different from the typical small-square form and the basketweave form (Fig. 1). However the reconstruction shows that the central Z-links that connect actin filaments of opposite polarity do in fact follow a basketweave course (Fig. 6, *b* and *c*). The appearance of the fish Z-band may be different because of the superimposed density of the polar links and because the Z-links are bulkier than those in images of typical basketweave Z-bands (Goldstein et al., 1979, 1987). In the latter the actin filaments in profile are circular- or square-shaped and their density is considerably greater than the connecting links as in Fig. 1 *c*. For the fish Z-band, the distinction between filament and link is less clear and together they have an extended shape. In a thin transverse section, the density of the Z-links relative to the actin filaments is probably greater in this muscle since the Z-band is only one layer thick.

To incorporate within a single Z-band model the appearances of the small-square lattice and the basketweave forms, Goldstein et al. (1979, 1982, 1987) envisage a dynamic structure of the Z-band in which the small-square lattice is the form in relaxed muscle and the transition to basketweave occurs upon activation. A systematic study of the muscle used in this work is required to investigate whether in different states of activation, the Z-band exhibits dynamic structural states including basketweave and small-square form.

Relationship to α-Actinin and Other Proteins

α-Actinin is known to be the major component (after actin) of the vertebrate muscle Z-band. Its presence in fish white muscle has been confirmed by antibody labeling (Luther, P., and T. Walliman, unpublished data). It is interesting to speculate how α-actinin fits in with the 3D structure of the fish Z-band. α-Actinin is known to be rod-shaped, 30–40 nm long and 3–4 nm in diameter (Suzuki et al., 1976). The actin-binding regions are believed to be at each end of the dimer (Blanchard et al., 1989). As noted in Results, each Z-link comprises three domains: a proximal domain of length 10 nm that runs up to the tip of one actin filament, a spanning domain 7 nm long and a distal domain about 15 nm long located in a region 5–20 nm from the end of an oppositely oriented filament. The length of such a link (~30–35 nm) is of the same order as an α-actinin dimer. A single α-actinin molecule may therefore form a link entirely. Each Z-link may be attached to the actin filament at the ends only, with the regions running along the filament in close proximity but not necessarily attached. Higher resolution data are required to resolve this further.

The polar link regions may be due to direct connections between α-actinin molecules along neighbouring actin fila-

ments. The connections could be due to additional proteins like amorphin as suggested by Chowrashi and Pepe (1982).

Casella et al. (1987) have shown the presence of an actin-capping protein located in the Z-band in skeletal muscle. Such a protein must form the terminal part of the actin filament in the reconstruction here. At the resolution of the work, there are no special features in the filament shaft density to show the presence of this protein.

Comparison with Recent Z-band Reconstructions

As mentioned earlier, a 3D reconstruction of the Z-band in honeybee flight muscle was recently published (Cheng and Deatherage, 1989; Deatherage et al., 1989). The insect Z-band differs fundamentally from the vertebrate Z-band since it is based on a hexagonal lattice. The overall symmetry was found to be P321. The bee Z-band comprises a central overlap region of 80 nm, equal to about two repeats of the actin filament. Five nonequivalent linking structures have been found. Four of these links are between pairs of oppositely oriented actin filaments. Each link has an axial component along the actin filament and a spanning component. Two links are located at the centre at the twofold symmetry positions of the lattice and are associated almost entirely with the sides of the actin filaments. The other two run from the end of one actin filament to the sides of the oppositely oriented filaments. These four links bear similarity to the fish Z-link as they all appear to have long attachment regions along the actin filaments. The fifth link connects three actin filaments of the same polarity with a threefold hub-shaped link.

More closely related to the fish Z-band is the new reconstruction of vertebrate nemaline rods (Z-crystals) by Morris et al. (1990). These are Z-bands greatly enlarged along the actin filament to form 3D crystalline structures. With the actin filaments from the adjacent sarcomeres overlapping the full width of the nemaline rod, the repeating unit of the Z-band comprises linkages between a pair of actin filaments of one polarity with a pair of actin filaments of the opposite polarity. Each linkage has three regions: a short transverse region attaching tangentially to the actin filament side, a long axial region running parallel to the actin filaments and a final transverse region linking across to the opposite polarity actin filament. The transverse regions of the like actin filaments appear to form a continuous link between the two filaments and may therefore be related to the polar links observed in the fish Z-band. All of the crosslinking structures in published Z-band or Z-crystal reconstructions thus show similarities. Higher resolution data will be needed to specify the α-actinin/actin interactions in more detail and to see if all of these Z-bands are related.

I wish to thank Dr. Ed Morris and Dr. J. M. Squire for many helpful discussions during the course of this work and Dr. R. A. Crowther for critical reading of the manuscript. I am grateful to the referees for their constructive comments to improve the manuscript.

This work was supported by a Leverhulme Trust award to Dr. J. M. Squire.

Received for publication 23 May 1990 and in revised form 7 February 1991.

References

Amos, L. A., R. Henderson, and P. N. T. Unwin. 1982. Three-dimensional structure determination by electron microscopy of two-dimensional crystals. *Prog. Biophys. Mol. Biol.* 39:183–231.

Blanchard, A., V. Ohanian, and D. Critchley. 1989. The structure and function of α-actinin. *J. Muscle Res. Cell Motil.* 10:280–289.

Casella, J. F., S. W. Craig, D. J. Maack, and A. E. Brown. 1987. Cap $Z_{(36/32)}$, a barbed end actin-capping protein, is a component of the Z-line of skeletal muscle. *J. Cell Biol.* 105:371–379.

Cheng, N., and J. F. Deatherage. 1989. Three-dimensional reconstruction of the Z disk of sectioned bee flight muscle. *J. Cell Biol.* 108:1761–1774.

Chowrashi, P. K., and F. A. Pepe. 1982. The Z-band: 85,000-dalton amorphin and alpha-actinin and their relation to structure. *J. Cell Biol.* 94:565–573.

Deatherage, J. F., N. Cheng, and B. Bullard. 1989. Arrangements of filaments and cross-links in the bee flight muscle Z disk by image analysis of oblique thin sections. *J. Cell Biol.* 108:1775–1782.

Egelman, E. H., N. Francis, and D. J. DeRosier. 1982. F-actin is a helix with a random variable twist. *Nature (Lond.).* 298:131–135.

Franzini-Armstrong, C. 1973. The structure of a simple Z-line. *J. Cell Biol.* 58:630–642.

Goldstein, M. A., J. P. Schroeter, and R. L. Sass. 1979. The Z-lattice in canine cardiac muscle. *J. Cell Biol.* 83:187–204.

Goldstein, M. A., J. P. Schroeter, and R. L. Sass. 1982. The Z-band lattice in a slow skeletal muscle. *J. Muscle Res. Cell Motil.* 3:333–348.

Goldstein, M. A., L. H. Michael, J. P. Schroeter, and R. L. Sass. 1987. Z-band dynamics as a function of sarcomere length and the contractile state of muscle. *FASEB (Fed. Am. Soc. Exp. Biol.) J.* 1:133–142.

Goll, D. E., F. H. M. Mommaerts, M. K. Reedy, and K. Seraydarian. 1969. Studies on α-actinin-like proteins liberated during trypsin digestion of α-actinin and of myofibrils. *Biochim. Biophys. Acta.* 175:174–194.

Huxley, H. E., and W. Brown. 1967. The low-angle X-ray diagram of vertebrate striated muscle and its behaviour during contraction and rigor. *J. Mol. Biol.* 30:383–434.

Kinnamon, J. C. 1989. Three-dimensional reconstruction from serial sections using the IBM PC. *Eur. J. Cell Biol.* 48:(Suppl.)25:65–68.

Knappeis, C. G., and F. Carlsen. 1962. The ultrastructure of the Z-disc in skeletal muscle. *J. Cell Biol.* 13:323–335.

Luther, P. K. 1989. Three-dimensional reconstruction of the Z-line in fish muscle. *Eur. J. Cell Biol.* 48:(Suppl.)25:153–156.

Luther, P. K., and R. A. Crowther. 1984. Three dimensional reconstruction from tilted sections of fish muscle M-band. *Nature (Lond.).* 307:566–568.

Luther, P. K., M. C. Lawrence, and R. A. Crowther. 1988. A method for monitoring the collapse of plastic sections as a function of electron dose. *Ultramicroscopy.* 24:7–18.

Macdonald, R. D., and A. G. Engel. 1971. Observations on organization of Z-disk components and on rod-bodies of Z-disk origin. *J. Cell Biol.* 48:431–437.

Morris, E. M., G. Nneji, and J. M. Squire. 1990. The three-dimensional structure of the nemaline rod Z-band. *J. Cell Biol.* 111:2961–2978.

Munro, P. M. G. 1986. Comparative ultrastructure of red and white muscle fibres of roach. Ph.D. thesis, University of London.

Rome, L. C., R. P. Funke, R. M. Alexander, G. Lutz, H. Aldridge, and F. Scott. 1988. Why animals have different muscle fibre types. *Nature (Lond.).* 335:824–827.

Rowe, R. W. D. 1973. The ultrastructure of the Z discs from white, intermediate, and red fibers of mammalian striated muscle. *J. Cell Biol.* 57:261–277.

Suzuki, A., D. E. Goll, I. Singh, R. E. Allen, R. M. Robson, and M. H. Stromer. (1976). Some properties of purified skeletal muscle α-actinin. *J. Biol. Chem.* 251:6860–6870.

Yamaguchi, M., R. M. Robson, M. H. Stromer, N. R. Cholvin, and M. Izumimoto. 1983. Properties of soleus muscle Z-lines and induced Z-line analogs revealed by dissection with Ca^{2+}-activated neutral protease. *Anat. Rec.* 206:345–362.

Yamaguchi, M., M. Izumimoto, R. M. Robson, and M. H. Stromer. 1985. Fine structure of wide and narrow vertebrate muscle Z-lines. *J. Mol. Biol.* 184:621–644.